PCCP

Cite this: *Phys. Chem. Chem. Phys.*, 2011, **13**, 19970–19978

www.rsc.org/pccp

PAPER

Water under temperature gradients: polarization effects and microscopic mechanisms of heat transfer

Jordan Muscatello,[a] Frank Römer,[a] Jonás Sala[ab] and Fernando Bresme*[a]

Received 10th June 2011, Accepted 27th September 2011
DOI: 10.1039/c1cp21895f

We report non-equilibrium molecular dynamics simulations (NEMD) of water under temperature gradients using a modified version of the central force model (MCFM). This model is very accurate in predicting the equation of state of water for a wide range of pressures and temperatures. We investigate the polarization response of water to thermal gradients, an effect that has been recently predicted using Non-Equilibrium Thermodynamics (NET) theory and computer simulations, as a function of the thermal gradient strength. We find that the polarization of the liquid varies linearly with the gradient strength, which indicates that the ratio of phenomenological coefficients regulating the coupling between the polarization response and the heat flux is independent of the gradient strength investigated. This notion supports the NET theoretical predictions. The coupling effect leading to the liquid polarization is fairly strong, leading to polarization fields of $\sim 10^{3-6}$ V m^{-1} for gradients of $\sim 10^{5-8}$ K m^{-1}, hence confirming earlier estimates. Finally we employ our NEMD approach to investigate the microscopic mechanism of heat transfer in water. The image emerging from the computation and analysis of the internal energy fluxes is that the transfer of energy is dominated by intermolecular interactions. For the MCFM model, we find that the contribution from hydrogen and oxygen is different, with the hydrogen contribution being larger than that of oxygen.

1 Introduction

Temperature gradients can result in strong coupling effects.[1,2] It is well known that particles in aqueous solutions move as a response to an imposed temperature gradient.[3,4] This is the so called Soret effect, also known as thermophoresis.[1] This effect is also observed in binary mixtures[5] and it has been used to separate isotopic mixtures. The thermoelectric response, namely charge transport induced by a temperature gradient, is the basis of a wide range of thermoelectric devices, which can convert waste heat into electricity.[6] An analog of this thermoelectric phenomenon is also observed in aqueous solutions. Here the charge carriers are ions. The temperature gradients lead to salinity gradients, which can in turn modify the thermophoretic response of large colloidal particles.[7] It has been recently discussed that similar thermoelectric phenomena are exploited by sharks to sense temperature gradients.[8] The thermoelectric material in this case is a gel, containing salt and water. This thermoelectric mechanism would provide sharks with a natural device to detect temperature changes in the surroundings without the intervention of ion channels.

The relevance of water as a medium to enable many of the non-equilibrium phenomena discussed above is obvious. However it is not so obvious how a complex liquid such as water behaves under the non-equilibrium conditions imposed by thermal gradients, and how heat is transferred through the liquid. Our microscopic understanding of the non-equilibrium response of water is still poor. Most works to date have been devoted to equilibrium studies. A significant number of these equilibrium investigations have been performed using computer simulations. These studies show that relatively simple models can explain the enormous complexity of the phase diagram of water and ice from a truly microscopic perspective.[9] These models have also helped to uncover new physical phenomena at low temperatures,[10,11] and to understand the complex interfacial behavior of water,[12–17] which is so relevant to explain the role that water plays in tuning the interactions between hydrophobic and hydrophilic surfaces.

We have recently explored the behavior of water under thermal gradients.[18] Using non-equilibrium molecular dynamics simulations of the Central Force Model of water,[19,20] we found that the water molecules tend to adopt a preferred orientation, with the dipole aligning with the gradient and the hydrogen atoms pointing preferentially towards the cold region,

[a] *Chemical Physics Section, Department of Chemistry, Imperial College London, The Thomas Young Centre and London Centre for Nanotechnology, SW7 2AZ, London, UK. E-mail: f.bresme@imperial.ac.uk*
[b] *Departament de Fsica i Enginyeria Nuclear, Universitat Politcnica de Catalunya, B4-B5 Campus Nord, 08034 Barcelona, Spain*

i.e., the temperature gradient polarizes the liquid. To the best of our knowledge this represents the first observation of such effect in a liquid, *i.e.*, an isotropic medium. We note that Lehmann reported shortly after the discovery of liquid crystals that temperature gradients can induce uniform rotation in liquid crystals, *i.e.*, in an *anisotropic* material.[21] Temperature induced polarization effects in liquid crystals have also been discussed more recently.[22]

Our initial investigations of water polarization under thermal gradients indicated that large gradients can induce a significant polarization, equivalent to an electrostatic field of $\sim 10^5$ V m^{-1} for a gradient of $\sim 10^7$ K m^{-1}. These temperature gradients are huge for macroscopic standards. However, gradients of this magnitude are easily achievable at micron and nanoscales. As a matter of fact gradients of the order of 10^6 K m^{-1}, 1 K μm^{-1} can be routinely obtained in experiments where colloidal particles are heated with lasers.[4] Despite these large gradients, recent experiments on colloidal suspensions[3] suggest, and theoretical analysis argues,[23] that the behavior of these suspensions under thermal gradients can be described using local thermodynamic equilibrium. This idea has been tested before using computer simulations, where much larger gradients are achievable. Analysis of the equation of state of fluids and liquids from these simulations, a notion that we exploit in this paper, did not reveal significant deviations from the equation of state obtained at equilibrium.[24,25]

In this paper we extend our investigations of water under temperature gradients to (1) investigate the influence of the temperature gradient strength on the water polarization, (2) test whether this dependence is consistent with the predictions of Non-Equilibrium Thermodynamics theory and (3) analyze the heat transport mechanism in liquid water by computing the oxygen and hydrogen contributions to the energy flux.

The article is structured as follows. Firstly, we set the problem from the perspective of the theory of Non-Equilibrium Thermodynamics. The methodological details, simulation method and force-field follow. We then present and discuss our results on the behavior of water under thermal gradients. A final section containing the main conclusions and final remarks closes the paper.

2 Non-equilibrium thermodynamics

We are interested in the investigation of the non-equilibrium response of an *isotropic* polar fluid to a temperature gradient. The phenomenological equations defining coupling effects between polarization and temperature gradients can be derived using Non-Equilibrium Thermodynamics theory.[1,18,26] The polarization induced by the temperature gradient is described in terms of two linear flux–force relations,

$$\frac{\partial \boldsymbol{P}}{\partial t} = -\frac{L_{\mathrm{pp}}}{T}(\boldsymbol{E}_{\mathrm{eq}} - \boldsymbol{E}) - \frac{L_{\mathrm{pq}}}{T^2}\nabla T \qquad (1)$$

$$\boldsymbol{J}_{\mathrm{q}} = -\frac{L_{\mathrm{qp}}}{T}(\boldsymbol{E}_{\mathrm{eq}} - \boldsymbol{E}) - \frac{L_{\mathrm{qq}}}{T^2}\nabla T \qquad (2)$$

where $\boldsymbol{P}$ is the polarization, $\boldsymbol{E}_{\mathrm{eq}}$ is the equilibrium electrostatic field, $\boldsymbol{E}$ is the electrostatic field in the sample, $\boldsymbol{J}_{\mathrm{q}}$ is the heat flux and $L_{\alpha\beta}$ are the phenomenological coefficients. One equation that defines the dependence of the electrostatic field $\boldsymbol{E}$ with the temperature gradient ∇T has been derived in ref. 18,

$$\boldsymbol{E} = \left(1 - \frac{1}{\varepsilon_r}\right)\frac{L_{\mathrm{pq}}}{L_{\mathrm{pp}}}\frac{\nabla T}{T}, \qquad (3)$$

which defines the electrostatic field in terms of the dielectric constant of the liquid ε_r. Eqn (3) shows that the polarization of the sample ($\boldsymbol{P} = -\varepsilon_0\boldsymbol{E}$) will reach a maximum value when $\varepsilon_r \to \infty$. However, the functional form of eqn (3) shows that the polarization varies rapidly with ε_r, and for high polar liquids such as water ($\varepsilon_r = 78$ at 298 K) it should be close to the maximum value for given ∇T, T and the $L_{\mathrm{pq}}/L_{\mathrm{pp}}$ ratio.

In this paper we will perform a systematic test of eqn (3) by simulating water at different temperature gradients.

3 Methodology

3.1 Modified central force model

In all the simulations the Modified Central Force Model (MCFM) of water was used.[20,27] This is a flexible three site model with partial charges on the hydrogens and oxygens calculated to reproduce the correct dipole moment of water in the gas phase. The intermolecular interactions in the MCFM follow the functional form introduced by Lemberg and Stillinger,[19] and the intramolecular interactions are modelled using harmonic potentials as introduced in ref. 20 and 27. Other implementations of this model have been proposed. Guillot and Guissani used a closely related model as a reference to include quantum effects through the Feynman–Hibbs formalism.[28]

The MCFM potential is characterised by the sum of intramolecular and intermolecular contributions $U_{\mathrm{intra},\alpha,\beta}(r)$ and $U_{\mathrm{inter},\alpha,\beta}(r)$ mediated by a switching function $t(r)$, such that,

$$U_{\alpha\beta}(r) = U_{\mathrm{intra},\alpha\beta}(r)[1 - t_{\alpha\beta}(r)] + U_{\mathrm{inter},\alpha\beta}(r)t_{\alpha\beta}(r) \qquad (4)$$

where $t_{\alpha\beta}$ is given by

$$t_{\alpha\beta} = \frac{1}{2}\left[1 + \tanh\left(\frac{r - R_{\alpha\beta}}{w_{\alpha\beta}}\right)\right] \qquad (5)$$

where $R_{\alpha\beta}$ and $w_{\alpha\beta}$ define the location and the transition from the intra to the intermolecular potential. Following ref. 20 we use, $R_{\mathrm{OH}} = 1.45$ Å, $R_{\mathrm{HH}} = 1.88$ Å, $w_{\mathrm{OH}} = 0.02$ Å and $w_{\mathrm{HH}} = 0.02$ Å. The oxygen–oxygen, oxygen–hydrogen and hydrogen–hydrogen intermolecular contributions are given by:

$$U_{\mathrm{inter,OO}}(r) = \frac{23700}{r^{8.8591}} - 0.25\exp[-4(r-3.4)^2] - 0.20\exp[-1.5(r-4.5)^2] + \frac{Z_O^2 e^2}{4\pi\varepsilon_0 r} \qquad (6)$$

$$U_{\mathrm{inter,OH}}(r) = \frac{-4}{1+\exp[5.49305(r-2.2)]} + \frac{Z_O Z_H e^2}{4\pi\varepsilon_0 r} \qquad (7)$$

$$U_{\mathrm{inter,HH}}(r) = \frac{Z_H^2 e^2}{4\pi\varepsilon_0 r} \qquad (8)$$

with $Z_{\mathrm{H}} = 0.32983e$ and $Z_{\mathrm{O}} = -2Z_{\mathrm{H}}$. The energies for all the potential functions are given in kcal mol^{-1} and distances in Å.

The intramolecular contributions are given by,

$$U_{\text{intra},\alpha\beta} = \frac{1}{2}k_{e,\alpha\beta}(r - r_{e,\alpha\beta})^2 + \frac{Z_\alpha Z_\beta}{4\pi\varepsilon_0 r} \quad (9)$$

where the equilibrium distance, r_e, and the force constant k_e are defined by,

$$r_{e,\alpha\beta} = r_{b,\alpha\beta} - \frac{Z_\alpha Z_\beta e^2}{4\pi\varepsilon_0 k_{b,\alpha\beta} r_{b,\alpha\beta}^2} \quad (10)$$

$$k_{e,\alpha\beta} = k_{b,\alpha\beta} - \frac{2Z_\alpha Z_\beta}{4\pi\varepsilon_0 r_{b,\alpha\beta}^3} \quad (11)$$

with $r_{b,OH}$ = 0.9584 Å, $r_{b,HH}$ = 1.5151 Å, $k_{b,OH}$ = 1147.6 kcal (mol Å^2)$^{-1}$ and $k_{b,OH}$ = 257.3 kcal (mol Å^2)$^{-1}$. The bond lengths, r_e, and the force constants, k_e, are adjusted in this way to reproduce the geometry of the water molecule in the vapour phase.[20,27]

3.2 Computational details

Non-equilibrium molecular dynamics simulations were performed using a rectangular box with dimensions $\{L_x,L_y,L_z\}$ = $\{5,1,1\} \times L_z$, where L_z = 19.725 Å, containing 1280 water molecules. The cell was divided into 120 layers along the x-axis to enable the evaluation of local system properties. The Wolf method was employed to compute the electrostatic interactions.[29,30] As we will see below this method offers a good trade off between computational efficiency and accuracy in the computation of bulk properties. The computations were performed with a cut-off of 9.8 Å and a convergence parameter of αL_x = 5.6.

In order to set up a thermal gradient in the system, the heat exchange algorithm (HEX) was used.[31] In this method, the ends and middle layers of the system cell act as heat sources/sinks, by periodically thermostatting the particles contained in the layers and thus setting up a heat flux $\pm\boldsymbol{J}_U$ in the system. By symmetry the fluxes in the two halves of the system cell have opposite direction, rendering a simulation box that is fully periodic. Kinetic energy is added to the molecules in the hot layers, and removed from the cold layers, such that the temperature at the hot and cold layers corresponds to T_H and T_C respectively. The momentum in the simulation box is conserved, retaining no net mass flow in the system. This arrangement is shown schematically in Fig. 1.

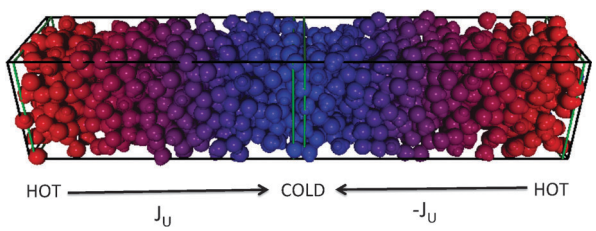

Fig. 1 Snapshot of a representative simulation showing the heat flux along the simulation box. The color scale indicates the local temperature of the water molecules. Simulation box dimensions $\{x,y,z\}$ = {19.725, 19.725, 98.625} Å. The location of the hot (425 K) and cold (225 K, middle of the box) thermostats is also shown.

In the stationary state a heat flux is set up in the system. The heat flux can be quantified through a microscopic expression, first derived by Irving and Kirkwood,[32] and extended to ionic systems in ref. 25,

$$\begin{aligned}\boldsymbol{J}_{U,\text{TOT}}(l) &= \boldsymbol{J}_{U,\text{KIN.}}(l) + \boldsymbol{J}_{U,\text{POT.}}(l) + \boldsymbol{J}_{U,\text{COL.}}(l) \\ &= \frac{1}{2V}\sum_{i=1}^{N\in l} m_i(\boldsymbol{v}_i - \boldsymbol{v})^2(\boldsymbol{v}_i - \boldsymbol{v}) + \frac{1}{V}\sum_{i=1}^{N\in l}\phi_i((\boldsymbol{v}_i - \boldsymbol{v}) \\ &\quad - \frac{1}{2V}\sum_{i=1}^{N\in l}\sum_{j\neq i}^{N}[(\boldsymbol{v}_i - \boldsymbol{v})\cdot F_{ij}]r_{ij}\end{aligned} \quad (12)$$

which gives the flux in a test volume of volume V located at layer l. m_i and $\boldsymbol{v}_i$ are the mass and velocity of particle i, respectively, ϕ_i is the potential energy of particle i, F_{ij} is the force between particles i and j at distance r_{ij} and $\boldsymbol{v}$ is the barocentric velocity, which in our simulations is zero as the net momentum of the simulation box is also zero. We note that the $\boldsymbol{J}_{U,\text{TOT}}(l)$ should be constant in the present simulations. This is true outside the thermostat layers. In that region $\boldsymbol{J}_{U,\text{TOT}}(l)$ features a plateau (see below). We use this plateau to estimate the energy flux in the gradient direction, $\boldsymbol{J}_{U,f}$.

In addition, the heat flux can be estimated by using the following continuity equation,

$$\boldsymbol{J}_{U,c} = \left\{\pm\frac{\Delta U}{2\delta t A}, 0, 0\right\} \quad (13)$$

where A is the cross-sectional area of the simulation cell, ΔU is the energy removed(−)/added(+) to the cold/hot layers, and δt is the time step, which was set to 0.3 fs in order to ensure good numerical stability in the integration of the fast intramolecular degrees of freedom.

The simulations involved an initial equilibration period of 45 ps to reach a temperature of 325 K across the whole system cell, and a further 45 ps of nonequilibrium simulation in order for the system to reach the stationary state. The results

Table 1 Summary of the systems simulated in this work. $J_{U,f}$ and $J_{U,c}$ correspond to the average flux obtained from eqn (12) and (13) respectively. ∇T represents the average temperature gradient over the whole simulation cell, and $\nabla T_{T=325\text{ K}}$ the local gradient at T = 325 K. The averages and uncertainties reported for the pressure were obtained from an ensemble average over the whole simulation box, and the uncertainty for $J_{U,f}$ was estimated from the analysis of the flux profiles reported in Fig. 6

ΔT/K	∇T/(K Å^{-1})	$\nabla T_{T=325\text{ K}}$/(K Å^{-1})	P/bar	$J_{U,f}$/(W m^{-2})	$J_{U,c}$/(W m^{-2})	$\rho_{T=325\text{ K}}$/(g cm^{-3})	$\lvert E_{x,T=325\text{ K}}\rvert$/(10^8 V m^{-1})
300–350	1	1.06 ± 0.06	308.5 ± 3.4	8.3 ± 0.2 × 10^9	8.04 ± 0.73 × 10^9	1.0001	2.79 ± 0.9
275–375	2	2.01 ± 0.06	351.3 ± 5.3	1.57 ± 0.02 × 10^{10}	1.49 ± 0.06 × 10^{10}	1.003	6.07 ± 1.2
250–400	3	2.92 ± 0.05	416 ± 3.5	2.26 ± 0.01 × 10^{10}	2.22 ± 0.06 × 10^{10}	1.004	8.34 ± 0.6
225–425	4	3.88 ± 0.05	495.6 ± 7.6	2.97 ± 0.02 × 10^{10}	2.84 ± 0.06 × 10^{10}	1.008	13.49 ± 0.6
325–475	3	—	1354 ± 10	2.46 ± 0.03 × 10^{10}	2.34 ± 0.1 × 10^{10}	—	—
250–350	2	1.93 ± 0.08	120 ± 11	1.4 ± 0.02 × 10^{10}	1.6 ± 0.1 × 10^{10}	0.9919	6.2 ± 1.2

presented below were obtained from 4–10 simulation runs consisting of 10^6 molecular dynamics steps, spanning a total of 1.5–3.0 ns. These simulations were used to estimate averages and statistical errors. A summary of all the simulations performed in this work is given in Table 1.

4 Results

4.1 Equation of state and thermal conductivity

Before we discuss our results for water polarization, we analyze the accuracy of the MCFM model in predicting the equation of state and thermal conductivity of water for different pressure and temperature conditions (see Table 1). The NEMD method preserves mechanical equilibrium, *i.e.*, the pressure along the box is constant (see Fig. 2, top panel). For each of these average pressures, the system develops temperature and density gradients. The analysis of these pairs of quantities at specific regions in the cell, along with the hypothesis of local equilibrium (see *e.g.* ref. 25 for an investigation considering ionic and non polar fluids), provides a route to construct the equation of state at specific isobars using a *single* simulation. The non-equilibrium simulated equation of state is compared with the corresponding experimental data in Fig. 2. We performed a running average over 2–4 consecutive layers to represent these data and in order to reduce the noise associated to the volume used to sample the densities along the simulation box. The different isobars were obtained from individual non-equilibrium simulations, at different pressure and different gradients, *i.e.*, covering several temperature intervals (see Table 1). The agreement with experimental results is excellent at the lower pressures investigated here <500 bars. The accuracy is comparable to that of two of the most popular force-fields of water TIP4P-2005[33] and SPC/E,[34] which model the water molecule as a rigid triangle.† The MCFM model correctly predicts the large change in density associated to the increase in temperature and pressure. At very high pressures, $\sim$1.3 kbar, it shows good agreement with the experiment at high temperatures (450 K) and deviates from the experiment, about 1%, at lower temperatures (350 K). This region of the phase diagram has been traditionally less investigated *via* computer simulations, although data using the TIP4P-2005 have been reported very recently.[35] At high pressures, the TIP4P-2005 model shows excellent agreement with the experimental equation of state, whereas the SPC/E model slightly underestimates the pressure at higher temperatures. Overall the level of accuracy of the MCFM and the SPC/E is comparable at this pressure, with the SPC/E performing better at low temperatures and the MCFM better at higher temperatures.

In the following we discuss our results for the thermal conductivity (TC) of the MCFM model. The TC can be obtained from Fourier's law, $\boldsymbol{J}_q \equiv \boldsymbol{J}_{U,c} = -\lambda\nabla T$, where $\boldsymbol{J}_q$ is the macroscopic heat flux, which is strictly equal to the computed internal energy flux, $\boldsymbol{J}_{U,c}$, in the absence of mass flux, *i.e.*, in our simulation conditions. In order to obtain better statistics the symmetry of the simulation cell was exploited by taking the average of each side about the point $L_x/2$, effectively "folding" the simulation cell in half. The thermal conductivity was then calculated for each layer in the "folded" cell, using the numerical derivative of the temperature profile (∇T) and the imposed heat flux, according to Fourier's Law stated above. We note that the local temperature gradient must be compatible with the local thermodynamic state defined by the pairs temperature/density at the constant pressure of the simulation. Hence, assuming a linear gradient for the whole temperature profile would provide only an average estimate of the thermal conductivity of the liquid. We have thus devised a strategy to extract the local thermal conductivity from our simulations. In all cases the thermal conductivity was obtained using the temperature gradient calculated from the temperature profile in the x-direction

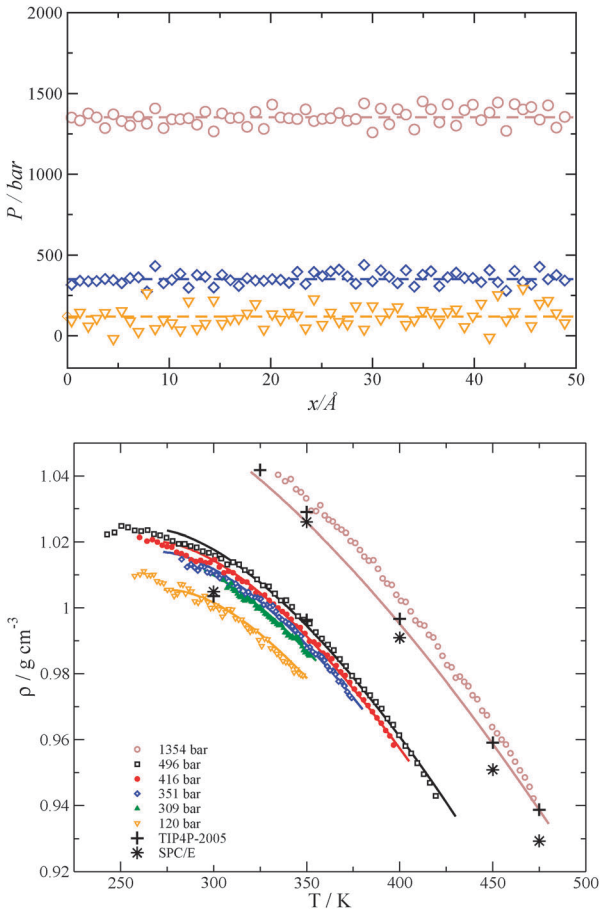

Fig. 2 (Top) Pressure profile along the simulation box for three different non-equilibrium simulations (the symbols have the same meaning as in Fig. 2, bottom). Dashed lines represent the average pressure for the whole simulation box. The pressure profile was obtained from the virial equation. (Bottom) Equation of state predicted by the MCFM of water at different pressures, obtained directly from the non-equilibrium molecular dynamics simulations. The symbols represent our simulations results and the lines experimental data.[36] Results from NPT simulations performed in this work for the TIP4P-2005[33] (crosses) and the SPC/E[34] (stars) models are also shown.

† The simulations for these two models were performed using molecular dynamics simulations in the isothermal–isobaric ensemble (N,P,T) with a potential cut-off in both cases of 9 Å and long range corrections for the pressure. The electrostatic interactions were computed using the Ewald summation method. The densities were obtained from averages over 2 ns.

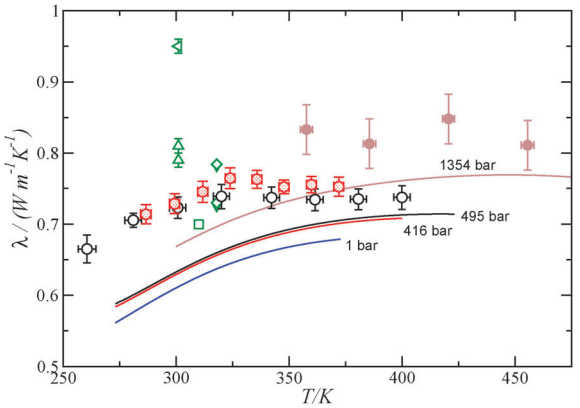

Fig. 3 Thermal conductivity of water as a function of temperature and pressure. Four different experimental isobars are represented: 1, 416, 495 and 1354 bars. Lines represent experimental data from ref. 36. Circles represent results from this work at 416 bar (shaded circles) 495 bar (open circles) and 1354 bar (filled circles). Open and filled diamonds represent simulation data for the thermal conductivity of the SPC/E and TIP4P models respectively.[38] Note that the results for these two models are very close to each other and they overlap almost completely in the figure. The square represents simulations of the flexible SPC/E model used in ref. 39. Open up-triangles represent non-equilibrium simulations of the SPC/E model (ref. 40), and the open left-triangle, non-equilibrium simulations of a fully flexible SPC/E model (see ref. 40 for details).

and the imposed heat flux calculated using the continuity equation. For each layer we calculated the local thermal conductivity using Fourier's Law. The fluctuations in the thermal conductivity are proportional to the size of the layer, being larger for a small layer. Hence we performed a running average of these thermal conductivities over several layers to reduce the fluctuations. The running averages were computed over 15 points. The error bars on each point represent the error in the temperature and thermal conductivity obtained from the analysis of the running average, and hence for a sub-volume of the non-equilibrium cell. We report 8 running averages for simulations performed with 10^7 time steps, and 4 for simulations with 4×10^6 time steps (see Fig. 3).

The thermal conductivity was then plotted as a function of the temperature in each layer. The error in T for each value is the standard error due to taking the average over a range of T values corresponding to an interval of 15 points in the data set. The error in λ is again the standard error of the mean plus the combined error on each data point in the averaging range. The thermal conductivity of water, as many other properties for this liquid, is anomalous.[37] It increases with temperature at low temperatures, unlike common liquids where the thermal conductivity decreases. This behavior has been traditionally explained as a signature of hydrogen bonding. At low temperature the hydrogen bonds can store energy resulting in an increase of thermal conductivity, whereas at high temperatures the hydrogen bond network is disrupted and water recovers the normal behavior observed in simple fluids.

Fig. 3 shows our results for the thermal conductivity. These are compared with the experimental data taken from ref. 36 and with previous simulation data obtained with forcefields that model water either as a rigid or flexible triangle.[38–40] We first note that the MCFM slightly overestimates the thermal conductivity of water at $\sim$300 K, by about 16%. This is within the same level of accuracy of water rigid models such as TIP4P and SPC/E. The fact that all these models, irrespective of their rather different functional forms, predict similar deviations might indicate that classical models are missing some degrees of freedom. Recent work by Vega *et al.*[41] has highlighted the importance of quantum nuclear effects in predicting the heat capacity of water. The heat capacity and the thermal conductivity are interlinked through the thermal diffusion factor, hence one can speculate such effects could also be relevant in the computation of thermal conductivities. In any case, current simulation methods do not allow a very precise determination of the thermal conductivity. This is well illustrated in our Fig. 3, which shows how the predictions from different authors/methods can differ between them by about 10–20%. Flexibility effects, namely molecular vibrations, may also play a role. This issue has been addressed by different authors,[40] by considering a flexible version of the SPC/E model that incorporates O–H vibrations. This model overestimates the thermal conductivity by 50%. This large value of thermal conductivity is in contrast with our results for the MCFM, which is also a flexible model, but predicts a thermal conductivity in much better agreement with experiment.

As discussed above the experimental thermal conductivity of water increases with temperature at low temperatures. This anomalous behaviour is reproduced by the MCFM (see Fig. 3 and also ref. 20), as shown in two independent isobars (see Fig. 3). This result shows that a classical treatment of the degrees of freedom would be enough to reproduce this anomalous property of water.

4.2 Water polarization

It has been recently shown that temperature gradients can induce molecular orientation in liquid water.[18] Because water is a polar molecule the alignment of the molecule dipole with the temperature gradient results in the polarization of the liquid. The Non-Equilibrium Thermodynamics realization of this notion is given in eqn (3). This equation shows that the resulting electrostatic field changes linearly with the temperature gradient, provided that the dielectric permittivity, the phenomenological coefficients and the temperature of the system are constants. One of us has used this equation to estimate the rate of the two coefficients L_{pq}/L_{pp}. This estimate opens a route to predict the polarization induced by experimentally achievable temperature gradients. In the following we take advantage of the wide range of simulations reported above to test eqn (3) against the simulation data. We have chosen simulations corresponding to four different isobars, where the largest difference in pressure between two isobars is 188 bars. For a fixed temperature, 325 K in this analysis, this change in pressure results in a very small change in liquid density, about 0.6%. This small change in density will have a small impact on the value of the dielectric permittivity appearing in eqn (3). Hence, the electrostatic field should depend linearly on the strength of the temperature gradient.

Fig. 4 shows the variation of the electric field between the hot and cold thermostats as a function of the temperature

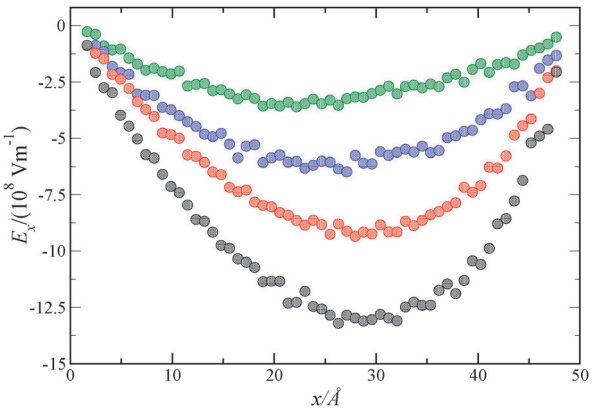

Fig. 4 The electric field profile along the x-direction as a function of the temperature gradient. From top to bottom, $\nabla T(K$ Å$^{-1}) = 1$ (309 bar), 2 (351 bar), 3 (416 bar) and 4 (496 bar). The hot and cold layers are located at $x \approx 0$ (hot) and $x \approx 49$ (cold) Å.

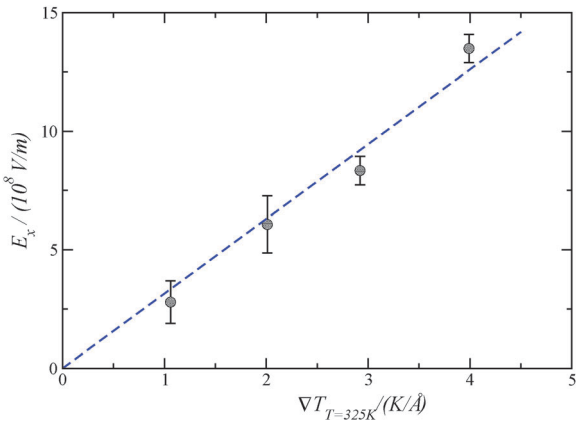

Fig. 5 Variation of the electrostatic field of water with the strength of the temperature gradient at $T = 325$ K. (Circles) NEMD simulations at 308.5 < P/bar < 495.6 (see Table 1). The line represents a linear fit to the NEMD simulation data imposing $E_x = 0$ at $\nabla T_{T=325\ \mathrm{K}} = 0$.

gradient strength at $T = 325$ K. The sign and strength of the electrostatic fields reported in Fig. 4 agree with previous work[18] and show, firstly, that the polarization of the MCFM water model is significant, and secondly that the hydrogen atoms are pointing towards the cold layer. The origin of the parabolic shape observed in the electrostatic field has been discussed before. It is connected to the NEMD simulation set up, with the cold thermostat in the center and two hot thermostats at the edges of the simulation box.‡ By symmetry the electrostatic fields on the left and on the right of the cold layer must have opposite sign. Hence the field must become zero at the cold and hot thermostats. The proximity between the cold and the hot layers imposes the parabolic shape. It was shown in ref. 18 that this effect can be reduced by elongating the box in the direction of the temperature gradient. We note that the value of the electrostatic field at the minimum depends very little on the box length. Hence we have chosen for our analysis a temperature, 325 K, which corresponds to a layer lying approximately in that minimum.

To test eqn (3) we have represented the electrostatic fields *versus* the temperature gradient strength. Our results for the electrostatic field are consistent with a linear dependence with the gradient strength (see Fig. 5 and Table 1 for numerical data) as predicted by eqn (3). A fitting of our data to this equation, using the fact that the field is zero at $\nabla T = 0$, gives 3.1×10^{-2} V K^{-1}. The dielectric constant of the MCFM at 300 K and 70 bar is 82. We expect that the dielectric constant at 325 K and the pressures considered in the non-equilibrium simulations will not be too different from this value. In fact, it is known from experiments that the dielectric constant of water shows a small dependence with pressure. At our temperature of interest, 325 K, the experimental dielectric constant varies from 70 (1 bar) to 75 (1500 bars).[42] Hence, considering this small dependence with pressure and our value for the dielectric constant it is clear that the dielectric constant contribution to the electrostatic field in eqn (3) will be very close to its maximum value, $(1 - \varepsilon_r^{-1}) \approx 1$. We can therefore estimate the ratio of the coefficients L_{pq}/L_{qq} directly from the slope 3.1×10^{-2} V K^{-1}, the temperature 325 K and eqn (3), ignoring the effect of the dielectric permittivity. The resulting value, $L_{pq}/L_{qq} \approx 10$ V agrees well with the first estimate of this quotient, 5–8 V, reported in ref. 18. As discussed in that paper the magnitude of this ratio indicates that strong temperature gradients 10^{5-8} K m^{-1}, which are achievable in micron and submicron scales, could generate polarization fields between 10^{3-6} V m^{-1}.

‡ Note that in Fig. 4 we are representing the electrostatic field for one half of the box only.

4.3 Energy fluxes

We investigate in this section the contributions to the internal energy flux. This discussion is important to understand the microscopic mechanism determining heat transfer in water. There has been a previous attempt to analyze this question by splitting the energy transfer in rotational and translational contributions.[43] Our approach is different, and relies on the definition of the internal energy flux given in eqn (12). Before we start our discussion we note that the energy fluxes computed using this equation are in good agreement (within the numerical uncertainties of the computations) with the continuity equation (see eqn (13)), showing that the NEMD simulations are consistent. Eqn (12) splits up the internal energy flux into two main contributions, one (collisional and potential energy terms) is defined by intermolecular interactions, whereas the other one (kinetic) is determined by transfer of kinetic energy. These flux contributions have been investigated before in non-equilibrium simulations of Lennard-Jones liquids and gases[31,44] as well as in molten salts.[25] These studies clearly showed the dependence of these different contributions on the nature of the phase considered. Naturally in gases, which involve large mean free paths, the kinetic contribution is dominant, whereas at densities characteristics of liquids, collisions between particles become relevant, and the collisional part is the dominant contribution to the energy flux. All these studies have shown that the potential contribution is small in both liquids and gases. Hence the analysis of the fluxes provides a simple interpretation of the heat transfer mechanism in terms of *two* main factors, kinetic and collisional. Fig. 6 shows our results for the fluxes at different temperature

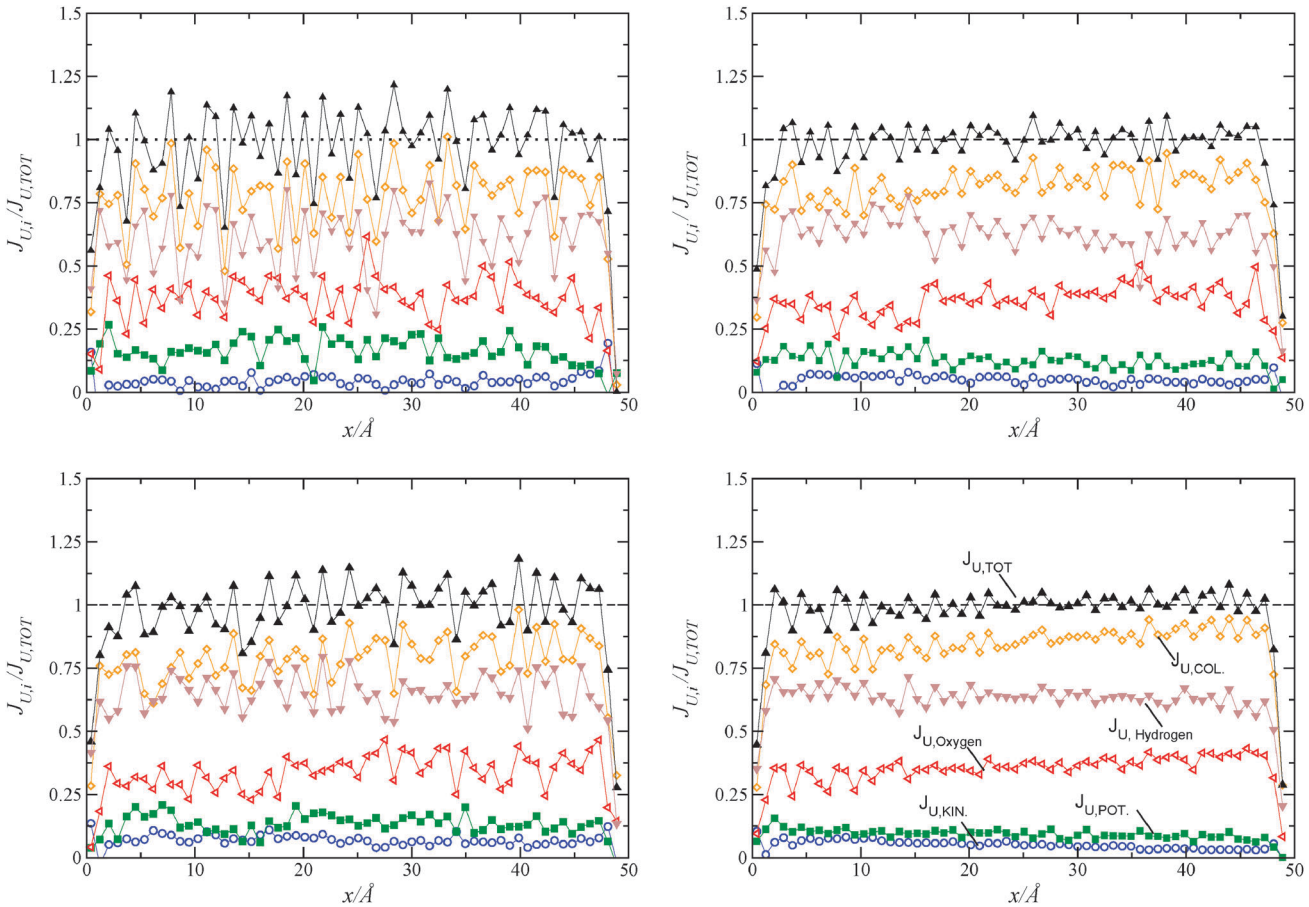

Fig. 6 Energy flux profiles for (clockwise from top left) (T_H, T_C) = (300, 350)K, P = 309 bar, (275, 375)K, P = 351.3 bar, (225, 425)K, P = 495.6 bar, and (325, 475)K, P = 1354 bar. The symbols represent the different contributions to the total flux: kinetic (circles), potential (squares), collisional (diamonds), total (triangle up), oxygen (triangle left) and hydrogen (triangle down). All the data were obtained using averages over 10^7 time steps, except for the (325–475) K system, where we used 4×10^6 steps.

gradients and different pressures. All the fluxes have been represented relative to the average value of the total energy flux (see $\boldsymbol{J}_{U,f}$ in Table 1 for numerical data). The noise in the data depends on the temperature gradient and the number of averages used in the computation. We have found that obtaining good averages for the energy fluxes requires a considerable computational effort. Our best set of data, (225,425) and P = 495.6 bars, were obtained over 3 ns (10^7 time steps). In the following we focus on these results as they provide a better view of the relative contributions and variation of the fluxes along the simulation box. For MCFM water we find that the main contribution to the energy flux is the collisional part, >75%. The potential contribution follows the trends reported in other systems. It is small and accounts for ~10% of the total energy flux only. The kinetic contribution is small and of the same order. The comparison of these three fluxes clearly shows that the main mechanism for heat transfer in the liquid is collisional. We find that the latter contribution increases from x = 0 to 50 Å, *i.e.*, from high to low temperatures/low to high densities, with a concomitant decrease from x = 0 to 50 Å in the kinetic contribution, *i.e.*, again from high to low temperatures. The other systems investigated follow similar trends regarding the relative dependence of the different contributions to the total energy flux.

We have also computed the individual atomic contributions to the energy flux, namely, how much of the energy is transported by oxygen and hydrogen atoms. Again the system, (225,425) and P = 495.6 bars, provides the best reference to analyze this question. Interestingly, for the MCFM model the hydrogen atom contribution to the energy flux is ~2 times larger than that of oxygen. This atomic contribution to heat transport depends on the thermodynamic conditions, and we find that it decreases/increases for hydrogen/oxygen as the temperature is reduced.

5 Conclusions and final remarks

We have performed non-equilibrium molecular dynamics simulations of water under thermal gradients. Water molecules were modeled through a modified version of the central force model (MCFM). This force-field models water as a fully flexible triangle, where the intramolecular vibrations and partial charges on the atoms are fitted to reproduce the properties of the water molecule in the vapor phase. Analysis of the non-equilibrium data provides a route to compute the equation of state of the liquid in a wide range of temperatures from a single simulation. We find that the MCFM is accurate in predicting the equation of state of water for a wide range of

pressures and temperatures. We have further computed the thermal conductivity at different thermodynamic conditions. The thermal conductivities at $\sim$300 K are overestimated by about 16%. This is in line with previous simulation results obtained with the TIP4P and SPC/E models, which represent water as a rigid triangle. The reason behind this overestimation of the thermal conductivity is unclear at the moment. Because our model, MCFM, is flexible, we may expect that the classical treatment of the vibrational degrees of freedom might have an impact on the computed thermal conductivities. Simulations of a rigid version of this model should provide a clue on whether the thermal conductivity of water can be accurately predicted using a classical approach or whether other degrees of freedom, *e.g.* nuclear effects, must be taken into account. This is a question that deserves further investigation.

The MCFM reproduces the anomalous increase of the thermal conductivity with temperature. This effect has been traditionally interpreted in terms of the temperature dependence of the energy stored in the hydrogen bond network. We have shown in this paper that such effect can be reproduced with a classical model. We also find that this classical model predicts an increase of the thermal conductivity with pressure in going from $\sim$400 bar to $\sim$1300 bar. We note that the current simulation approach and the current force-fields are not precise enough to observe clear trends for smaller pressure ranges, $\pm$100 bar.

We have investigated the response of liquid water to temperature gradients. Non-Equilibrium Thermodynamics (NET) predicts that a polar fluid should develop a polarization field as a response to an imposed thermal gradient.[18] Furthermore, at constant density and temperature the field should vary linearly with temperature. We have tested this idea by performing simulations of the liquid at different temperature gradient strengths. In agreement with previous work,[18] the MCFM water molecules orient with the dipoles pointing towards the cold region. We find that the degree of orientation and the resulting electrostatic field depend linearly on the gradient, as predicted by NET. This analysis provides an independent estimate of the ratio of the phenomenological coefficients, $L_{pq}/L_{pp} \approx 10$ V for the MCFM model, which is in good agreement with our previous results.[18] This ratio determines the strength of the polarization field. Strong gradients, 10^{5-8} K m^{-1}, should produce significant polarization effects 10^{3-6} V m^{-1}.

Finally, we have investigated the microscopic mechanism of heat transfer in water by analyzing the total energy flux contributions. The total energy flux can be split up into two main contributions. One of them is kinetic, whereas the second one measures the energy transfer through intermolecular interactions. We find that intermolecular interactions are the dominant, $>$75%, mechanism for heat transfer in water. This provides a simple microscopic interpretation, where the energy is transferred through collisions between the atomic sites. This collisional contribution includes all types of interactions, also hydrogen bonding. Given the role that hydrogen bonds play in defining many of the water properties, including the anomalous properties, it would be very interesting to analyze the net contribution of hydrogen bonds to the energy flux. We also find that the hydrogen atoms are more efficient in transporting heat. This asymmetry in the heat transfer ability of hydrogen *versus* oxygen must have a molecular origin, possibly connected to the molecular geometry of the MCFM water molecule. Further work is therefore needed to advance our knowledge on the relationship between heat transfer and molecular geometry to provide an unequivocal model to explain the microscopic mechanism of heat transport in water.

Acknowledgements

We would like to acknowledge the Imperial College High Performance Computing Service for providing computational resources. Financial support for this work was provided by The Leverhulme Trust and by the EPSRC through a DTA scholarship to JM. JS is a recipient of an FPI fellowship from the Ministerio de Educación y Ciencia (MEC) of Spain. FB would like to thank the EPSRC for the award of a Leadership Fellowship (EP/J003859/1).

References

1 S. R. de Groot and P. Mazur, *Non-Equilibrium Thermodynamics*, North-Holland, Amsterdam, 1962.
2 S. Kjelstrup and D. Bedeaux, *Non-Equilibrium Thermodynamics of Heterogeneous Systems*, World Scientific, Singapore, 2008.
3 S. Duhr and D. Braun, *Phys. Rev. Lett.*, 2006, **96**, 168301.
4 H.-R. Jiang, H. Wada, N. Yoshinaga and M. Sano, *Phys. Rev. Lett.*, 2009, **102**, 208301.
5 C. Debuschewitz and W. Köhler, *Phys. Rev. Lett.*, 2001, **87**, 055901.
6 G. J. Snyder and E. S. Toberer, *Nat. Mater.*, 2008, **7**, 105.
7 A. Würger, *Phys. Rev. Lett.*, 2008, **101**, 108302.
8 B. R. Brown, *Nature*, 2003, **421**, 495.
9 E. Sanz, C. Vega, J. L. F. Abascal and L. G. MacDowell, *Phys. Rev. Lett.*, 2004, **92**, 255701.
10 O. Mishima and H. E. Stanley, *Nature*, 1998, **396**, 329.
11 P. G. Debenedetti, *J. Phys.: Condens. Matter*, 2003, **15**, R1669.
12 L. R. Pratt and A. Pohorille, *Chem. Rev.*, 2002, **102**, 2671.
13 H. S. Ashbaugh, L. R. Pratt, M. E. Paulaitis, J. Clohecy and T. L. Beck, *J. Am. Chem. Soc.*, 2005, **127**, 2808.
14 F. Bresme, E. Chacón and P. Tarazona, *Phys. Rev. Lett.*, 2008, **10**, 4704.
15 J. Faraudo and F. Bresme, *Phys. Rev. Lett.*, 2004, **92**, 236102.
16 F. Bresme and A. Wynveen, *J. Chem. Phys.*, 2007, **126**, 044501.
17 T. G. Lombardo, N. Giovambattista and P. G. Debenedetti, *Faraday Discuss.*, 2009, **141**, 359.
18 F. Bresme, A. Lervik, D. Bedeaux and S. Kjelstrup, *Phys. Rev. Lett.*, 2008, **101**, 020602.
19 H. L. Lemberg and F. H. Stillinger, *J. Chem. Phys.*, 2001, **115**, 7564.
20 F. Bresme, *J. Chem. Phys.*, 2001, **115**, 7564.
21 O. Lehmann, *Ann. Phys.*, 1900, **307**, 649.
22 I. Jánossy, *Europhys. Lett.*, 1988, **5**, 431.
23 R. D. Astumian, *Proc. Natl. Acad. Sci. U. S. A.*, 2007, **104**, 3.
24 B. Hafskjold and S. Kjelstrup-Ratkje, *J. Stat. Phys.*, 1995, **78**, 463.
25 F. Bresme, B. Hafskjold and I. Wold, *J. Phys. Chem.*, 1996, **100**, 1879.
26 M. Marvan, *Czech. J. Phys.*, 1969, **19**, 1240.
27 F. Bresme, *J. Chem. Phys.*, 2008, **108**, 4505.
28 B. Guillot and Y. Guissani, *J. Chem. Phys.*, 1998, **108**, 10162.
29 D. Wolf, P. Keblinski, S. R. Phillpot and J. Eggebrecht, *J. Chem. Phys.*, 1999, **110**, 8254.
30 C. J. Fennell and J. D. Gezelter, *J. Chem. Phys.*, 2006, **124**, 234104.
31 T. Ikeshoji and B. Hafskjold, *Mol. Phys.*, 1994, **81**, 251.
32 J. H. Irving and J. G. Kirkwood, *J. Chem. Phys.*, 1950, **18**, 817.
33 J. L. F. Abascal and C. Vega, *J. Chem. Phys.*, 2005, **123**, 234505.
34 H. J. C. Berendsen, J. R. Grigera and T. P. Straatsma, *J. Phys. Chem.*, 1987, **91**, 6269.
35 J. L. F. Abascal and C. Vega, *J. Chem. Phys.*, 2011, **134**, 186101.
36 *Thermophysical Properties of Fluid Systems*, ed. P. Linstrom and W. Mallard, National Institute of Standards and Technology,

Gaithersburg MD, 2006, 20899, http://webbook.nist.gov, (retrieved May 29, 2011).
37 D. Eisenberg and W. Kauzmann, *The Structure and Properties of Water*, Clarendon Press, Oxford, 2005.
38 D. Bedrov and G. D. Smith, *J. Chem. Phys.*, 2000, **113**, 8080.
39 W. Evans, J. Fish and P. Keblinski, *J. Chem. Phys.*, 2007, **126**, 154504.
40 M. Zhang, E. Lussetti, L. E. S. de Souza and F. Müller-Plathe, *J. Phys. Chem. B*, 2005, **109**, 15060.
41 C. Vega, M. M. Conde, C. McBride, J. L. F. Abascal, E. G. Noya, R. Ramirez and L. M. Sesé, *J. Chem. Phys.*, 2010, **132**, 046101.
42 M. Uematsu and E. U. Franck, *J. Phys. Chem. Ref. Data*, 1980, **9**, 1291.
43 T. Ohara, *J. Chem. Phys.*, 1999, **111**, 6492.
44 B. Hafskjold and T. Ikeshoji, *Mol. Simul.*, 1996, **16**, 139.

